Crystal structure, hydrogen bonds, and lattice dynamics in kanemite from first-principles calculations

P. Piekarz,[1] M. Derzsi,[1,2] P. T. Jochym,[1] J. Łażewski,[1] M. Sternik,[1]
K. Parlinski,[1] and E. M. Serwicka[3]

[1]*Institute of Nuclear Physics, Polish Academy of Sciences, Radzikowskiego 152, PL-31342 Kraków, Poland*

[2]*Department of Theoretical Chemistry, Institute of Inorganic Chemistry, Slovak Academy of Sciences, Dúbravská cesta 9, SK-84536 Bratislava, Slovakia*

[3]*Institute of Catalysis and Surface Chemistry, Polish Academy of Sciences, Niezapominajek 8, PL-30329 Kraków, Poland*

(Received 15 December 2008; revised manuscript received 6 March 2009; published 6 April 2009)

The crystal structure and vibrational spectrum of kanemite ($NaHSi_2O_5 \cdot 3H_2O$) were studied using the density-functional theory. The calculations were carried out in a lower space group ($Pna2_1$) in order to eliminate the finite-temperature disordered configurations of protons in hydrogen bonds. It was found that the SiO_4 tetrahedra are linked by a short strong O-H$\cdots$O hydrogen bond with a single asymmetric potential well at low temperatures. Two energetically equivalent sites were obtained for the position of the H atom. Apart from the hydrogen bonds reported in earlier studies, additional moderate O-H$\cdots$O hydrogen bond was found to stabilize the hydrated Na layers within the silicon layers at low temperatures. The vibrational spectrum was analyzed in detail in the entire energy range (0–500 meV), focusing on the vibrations of hydrogen atoms. A perfect correlation appears to exist between the OH (stretching and torsional) frequencies and donor-acceptor distances of the respective hydrogen bonds.

DOI: 10.1103/PhysRevB.79.134105 PACS number(s): 61.50.Ah, 63.20.dk

I. INTRODUCTION

Kanemite belongs to the group of sodium silicate minerals. It is a naturally occurring mineral first found in Kanem, at the edge of the Lake Chad,[1] and identified at other places such as the Lovozero massif at Kola peninsula,[2] and in the sediments of Lake Bogoria in Kenya.[3] Kanemite can be synthesized in different ways from NaOH-SiO_2 mixtures, sodium silicate solutions, or by dehydration (rehydration) of other sodium silicates such as $Na_2Si_2O_5$, makatite, and magadiite.[4] The crystal structure consists of the hydrated sodium layers alternating with the SiO_4 layers. Similarly to other sodium silicates, kanemite can be easily modified due to its high inner-crystalline reactivity. Typical reactions such as the exchange of sodium atoms by organic cations and protons, reversible hydration and dehydration, ion exchange at surface, and intercalation of organic compounds are observed.[4–6] The intercalation processes have been used for the reconstruction of the crystal and synthesis of new materials with technological applications.[7] Due to the flexibility of its silicate layers, kanemite is used as the starting material for the synthesis of the mesoporous material FSM-16, with novel catalytic and absorption properties.[8–11]

The physical properties of kanemite are strongly determined by hydrogen bonds. Providing the cohesion force between sodium and silicon layers they stabilize the crystal structure at low temperatures. High reactivity and chemical changes observed with increasing temperature can be attributed to unique properties of hydrogen bonds and proton dynamics. Nuclear magnetic-resonance studies revealed an extensive hydrogen-bonding between water molecules and silicate layers.[5,12] Later, the existence of hydrogen bonds was confirmed in the x-ray diffraction study.[13] Since the neutron studies have not been performed for kanemite, the detailed and accurate information about the geometrical and dynamical properties of hydrogen bonds is still missing. The vibrational spectrum is partially known from the Raman and infrared studies.[14]

A fast progress in the calculation methods based on the *ab initio* density-functional theory (DFT) allows one to study structural and dynamical properties of more complex and larger systems. This approach has been successfully applied also to many molecular crystals including hydrogen bonded systems.[15–18] Kanemite has been studied theoretically by the molecular-dynamics (MD) simulations using the force field potentials.[19] This modeling provided some insight into the mechanism of water incorporation into the interlayer spaces and hydration energetics of kanemite. In this paper, we analyze in detail the crystal structure and the vibrational properties of kanemite focusing on the geometry and dynamics of hydrogen atoms using the DFT approach. The paper is organized as follows. In Sec. II, we describe the theoretical methods used in the crystal relaxation and phonon spectrum calculations. Section III contains the detailed information on crystal structure and hydrogen bonds. The vibrational properties of kanemite are discussed in Sec. IV and finally, the main conclusions are presented in Sec. V.

II. CALCULATION DETAILS

The crystal structure of kanemite was optimized by the minimization of the total energy within the DFT approach using the Vienna *Ab initio* Simulation Package (VASP).[20] The Kohn–Sham equations are solved by the iterative self-consistent procedure using the plane-wave basis set. The full-potential wave functions, charge densities, and interatomic interactions are obtained by the projector augmented-wave method.[21] For the exchange-correlation part of the Hamiltonian, the generalized gradient approximation (GGA) has been applied.[22] The following valence electron basis set

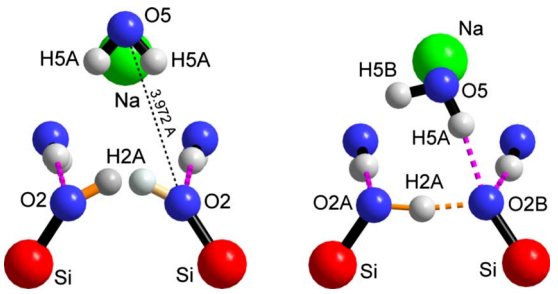

FIG. 1. (Color online) Comparison of hydrogen bonds geometry in the experimental (left) and theoretical (right) structures visualized in the *bc* plane and constrained by *Pbcn* and $Pna2_1$ space groups, respectively.

was chosen: $H:1s^1$, $O:2s^2p^4$, $Na:2p^63s^1$, and $Si:3s^23p^2$. To improve calculation accuracy the energy cutoff for the plane-wave expansion was increased to 500 eV. The summation over the Brillouin zone was done on the $4\times2\times4$ Monkhorst–Pack grid,[23] with the 18 irreducible *k* points.

The calculations were done with the periodic boundary conditions for two different sizes of the supercell. First, the lattice constants and atomic positions were optimized in the unit cell ($1\times1\times1$ supercell) with 72 atoms. Next, the size of the cell was doubled along the shortest edge (a =4.94 Å) and the crystal structure was reoptimized again. Atomic positions were relaxed using two procedures: the conjugate gradient and *quasi*-Newton methods.[20] The electronic and ionic optimizations were continued until the energy differences were less than 10^{-7} and 10^{-5} eV, respectively. At the end, the residual forces dropped below 10^{-4} eV/Å and simultaneously the residual hydrostatic pressure was smaller than 1 kb.

The optimized crystal was a starting point for the lattice dynamics studies. The phonon frequencies were computed with the method developed by Parlinski *et al.*[24] and incorporated into the PHONON program.[25] To determine the vibrational spectrum, the Hellmann–Feynman forces were generated by displacing—one by one—all nonequivalent atoms in *x*, *y*, and *z* directions by 0.03 Å. To minimize systematic errors, we displaced atoms in both positive and negative directions. The force constants and dynamical matrices were constructed using all the symmetry elements of the supercell. The vibrational frequencies and polarization vectors were obtained by the diagonalization of the dynamical matrix in the chosen set of *k* points.

III. STRUCTURAL ANALYSIS

A. Crystal parameters

According to the diffraction experiments the crystal structure of kanemite is orthorhombic with the space group *Pbcn*.[13,26] Two equivalent crystallographic sites were observed for the position of hydrogen H2A, occupying the space between two O2 atoms belonging to distinct silanol groups (Fig. 1, left). Taking into consideration the small separation of the two neighboring O2 atoms (2.488 Å), obviously only one hydrogen atom can occupy the space in between them, forming a very short hydrogen bond. In order to build our theoretical model of the kanemite structure, a single position of the hydrogen atom had to be chosen, which breaks the *Pbcn* symmetry (Fig. 1, right). Realizing, that in the unit cell, there are four such hydrogen atoms, we have chosen such a combination of the possible hydrogen positions, as to obtain the highest possible subgroup $Pna2_1$. This subgroup preserves four group elements out of eight ones present in *Pbcn*. The lowering of the space-group symmetry to $Pna2_1$ causes the increase of the number of nonequivalent atoms in the unit cell from 11 to 18 including seven H, eight O, two Si, and one Na atom. Additional calculations for the centrosymmetric subgroup $P2_1/c$ were also performed. Comparing the two sets of calculations, no considerable dependence of the lattice parameters and atomic positions on the crystal symmetry was observed. Therefore, we have chosen to present here the results obtained for the $Pna2_1$ space group only.

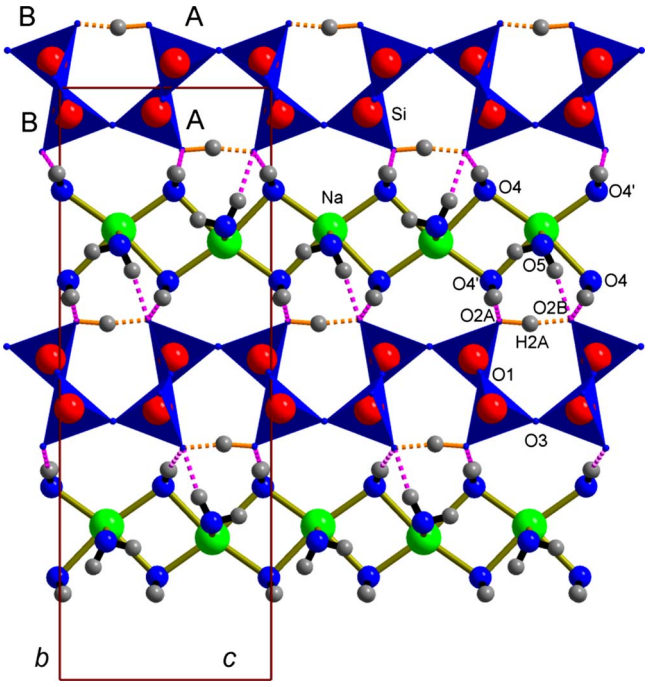

FIG. 2. (Color online) Low-temperature structure of kanemite shown in the *bc* plane as obtained from the present DFT calculations.

In Fig. 2 we show the optimized structure of kanemite and its unit-cell edges in the *bc* plane. It reproduces very well the characteristic features of the crystal known from the experiment[13,26] and summarized here shortly. It is built of silicon layers which are alternating with the layers formed by sodium ions coordinated by six water molecules. The silicon layers consist of connected SiO_4 tetrahedra forming six-member rings of SiO_4-$HOSiO_3$ units. The neighboring tetrahedra are connected by two bridging oxygen atoms, O1 and O3, and a hydrogen bond created between atoms O2A and O2B, intermediated by the hydrogen H2A. The sodium ions are coordinated by six water molecules in distorted octahedra. The sharing edges between the octahedra are formed by O4 ions. Along the *a* direction (out of plane of Fig. 2), the octahedra are connected by the corner sharing O5 ions. In

TABLE I. Comparison of calculated and experimental lattice constants and selected interatomic distances (in Å). A and B signs in brackets stand for the two different tetrahedra present in the theoretical structure.

Lattice constants	DFT-GGA	Expt. (293 K)
a	4.982	4.946[a,b]
b	20.784	20.502,[a] 20.510[b]
c	7.408	7.275,[a] 7.277[b]
Bond		Ref. 13
Si-O1	1.633(A)	1.612
	1.638(B)	
Si′-O1	1.635(A)	1.608
	1.639(B)	
Si-O2	1.641(A)	1.595
	1.619(B)	
Si-O3	1.616(A)	1.609
	1.642(B)	
Na-O4	2.377	2.403
	2.512	
	2.427	2.413
	2.492	
Na-O5	2.538	2.546
	2.557	

[a]Reference 13.
[b]Reference 26.

contrast to the experimental structure, where the building block of the silicon layers is one unique SiO_4 tetrahedra with four distinct Si-O bond lengths, two slightly different SiO_4 tetrahedra (A and B) are formed in the optimized model. They alternate along the *c* direction in such a way that atoms O3 and H2A always connect tetrahedron A with tetrahedron B. In the same time, atom O1 bridges two same (A or B) tetrahedra along the *b* direction.

In Table I the theoretical lattice parameters are compared to the experimental data obtained in diffraction measurements.[13,26] Our calculations overestimate the experimental values of *a*, *b*, and *c* by ≈0.7%, 1.3%, and 1.8%, respectively. The larger theoretical volume is typical for the GGA approximation. Therefore, also the theoretical interatomic distances in kanemite are in general larger than the experimental ones. In the second part of Table I, selected interatomic distances are summarized, comparing the calculated results to the single-crystal x-ray diffraction data obtained at room temperature.

In the experimental structure four Si-O bonds are present: Si-O1, Si′-O1, Si-O2, and Si-O3. Atom O1 is involved in two different Si-O bonds, connecting two neighboring tetrahedra (O_3Si-O1-[SiO_3]′). Atom O3 is also a bridging atom between two tetrahedra. Here, however, no Si′-O3 is distinguished because the two joined Si-O3 bonds are equivalent in the experimental structure. The four distinct Si-O bonding distances are caused by external potential formed by the crystal field and hydrogen bonds. Since, in the theoretical structure, two distinct SiO_4 tetrahedra are formed, two theoretical values (A and B) correspond to each experimental Si-O bond in Table I. On one hand, concerning the Si-O1 and Si′-O1 bonds, the two theoretical distances are very close to each other as well as to their respective experimental values. On the other hand, comparing the Si-O2 bond lengths in the A and B tetrahedra, the difference is by 1 order of a magnitude higher ($\Delta \approx 0.02$ Å) than in the case of Si-O1 and Si′-O1 bonds ($\Delta \approx 0.005$ Å). The same applies to Si-O3 bond lengths ($\Delta \approx 0.03$ Å) with respect to the Si-O1 and Si′-O1 bonds. Interestingly, very close values are obtained for Si-O2A (Si-O2B) and Si-O3B (Si-O3A) bonds.

Having a closer look at the two distinct tetrahedra, the main difference between them is that the tetrahedra A are always proton donors and the tetrahedra B proton acceptors in the O2A-H2A···O2B bond. It seems that the asymmetric position of the proton within this hydrogen bond causes the main differences between the A and B tetrahedra, namely, it influences the lengths of Si-O2 and Si-O3 bonds. In tetrahedra A, the Si-O2 bond is always a proton donor and in tetrahedra B, a proton acceptor to the O2A-H2A···O2B bond. Therefore, the formation of the asymmetric O2A-H2A···O2B bond causes the elongation of the donating Si-O2A bond and contraction of the acceptor Si-O2B bond. In the same time, Si-O3 contracts within the proton-donating A tetrahedra and elongates within the proton-accepting B tetrahedra. Since the differences between the A and B tetrahedra result from the asymmetric position of H2A atom, they cannot be observed in diffraction measurement, from which two crystallographically equivalent H2A sites are obtained. Therefore one cannot see which tetrahedra is the proton donor and which is the proton acceptor of the O2A-H2A···O2B bond, and only the statistical average of these two arrangements is observed.

The position of Na atom obtained in the calculations is slightly shifted (about 4%) in the *c* direction. The lowering of the crystal symmetry caused redistribution of all six water molecules coordinating the sodium atom in the distorted octahedra. Six interatomic Na···$O_{(H_2O)}$ distances are found in the optimized structure instead of three experimental ones (Table I). The position of the atom O5, connecting two octahedra in the *a* direction, shows the largest disagreement between theory and experiment. Its theoretical position is shifted by ≈11% along the *b* direction. As it will be discussed later, the water molecule H5A-O5-H5A changes its position in order to form the additional hydrogen bond O5-H5A···O2B (Fig. 1, right).

B. Hydrogen bonding

In kanemite, most of its hydrogen atoms are bound within the water molecules and create intermolecular O-H···O bonds (Fig. 3). The geometry of all hydrogen bonds, both experimental and theoretical, is presented in Table II. Since the x rays probe the electron charge density, the experimental positions of hydrogen atoms are determined only approximately. Therefore a good agreement between the experimental and theoretical geometries concerning the positions of hydrogen atoms may be fortunate. Determining the atomic positions from the electron density, x rays in general under-

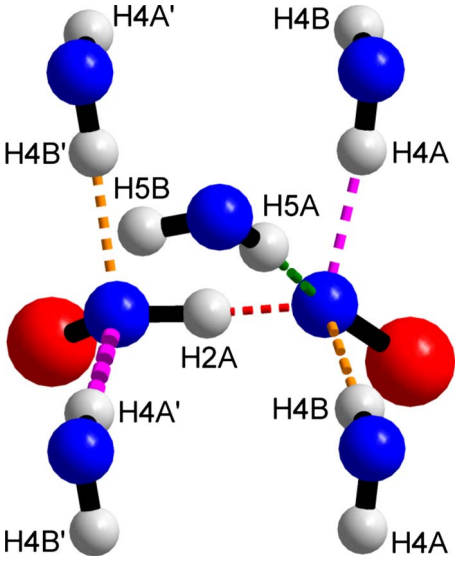

FIG. 3. (Color online) Hydrogen bonds in the optimized structure of kanemite.

estimate the O-H bonding distances. It is clearly seen in the H4A-O4-H4B water molecule, where the H-O distances are strongly underestimated. However, it should be noted that Garvie *et al.*[13] attributed these small distances to the high atomic displacements. Both hydrogen atoms, H4A and H4B, link O4 (donor) with O2 (acceptor) in the moderate hydrogen bonds. According to the experimental data, the structure of kanemite is stabilized by three distinct hydrogen bonds. Two moderate, O4-H4A···O2 and O4-H4B···O2, bonds connect the H4A-O4-H4B water molecule with the oxygen atoms in the SiO_4 tetrahedra, neighboring each other along the *a* direction. The same O2 atoms are involved in formation of a very short O2-H2A···O2 bond ($d_{O\cdots O}$=2.498 Å) along the *c* direction. This bond plays an important role in connecting the two SiO_4 tetrahedra, stabilizing them within the silicon layers. As discussed earlier, the diffraction study revealed two equivalent crystallographic sites (in the distance 0.77 Å) for the position of the H2A hydrogen atom in between the two neighboring O2 atoms. Our theoretical calculations also predict two energetically equivalent minima for the hydrogen atom position and thus agree with the experimental observations.

Because one H2A atom cannot sit at the same time at both crystallographically equivalent sites, the symmetry of the crystal must be locally broken. As a result, in the optimized structure, the geometries of the two adjacent H4A-O4-H4B water molecules, neighboring each other in the *c* direction, are modified by different potentials and are therefore no more equivalent. We introduce the "prime" sign in order to distinguish those water molecules (see Fig. 3). Obviously, two different water molecules will create distinct hydrogen bonds with the O2 atoms and, instead of two, four intermediate hydrogen bonds are distinguished in our theoretical structure (Table II). Our calculations reveal that at low temperatures the structure is further stabilized by additional hydrogen bond created between H5A from the H5A-O5-H5B water molecule and atom O2B from the SiO_4 tetrahedra (Fig. 1, right). This bond has not been identified in the diffraction studies. According to the calculations, at zero temperature the whole water molecule is shifted along *b* direction toward the O2A and O2B atoms, getting closer to O2B. As a result, the theoretical values obtained for O5-O2A (3.061 Å) and O5-O2B (2.797 Å) distances are much smaller than the experimental value *d*(O5-O2)=3.972 Å. The calculated H5A-O5-H5B angle (102.79°) corresponds much better to the water-molecule value (104.45°) than the measured one (83.04°). However, it was reported[13] that the measured value is wrong because of low accuracy of the hydrogen atoms maxima localization. In our structure the water molecule additionally rotates in the *bc* plane to be stabilized by a hydrogen bond to O2B atom. Interestingly, the new hydrogen bond created between atoms O2 and O5 can provide another link between the hydrated Na layer and the silicate tetrahedra. Previously only the O4-H4A···O2 and O4-H4B···O2 bonds were discussed as the potential candidates for the interlayer cohesion interaction.[13]

The presence of the two equivalent H2A sites suggests two possible solutions: the existence of double-well potential with the proton jumping (tunneling) between the two sites or statistical distribution of hydrogen atoms in both equivalent states. In order to resolve the question which case is in fact realized, we have calculated the effective one-dimensional potential of the hydrogen H2A along the bond O2A-H2A···O2B. At each hydrogen position, we have calculated total energy of the system with all other atoms kept fixed to their positions taken from the fully optimized struc-

TABLE II. Calculated and experimental (Ref. 13) bond distances (in Å) and angles (in degrees) in the hydrogen bonds of kanemite.

Donor-H···Acceptor		D-H	H-A	D-A	Angle (D-H···A)
O2A-H2A···O2B	DFT	1.075	1.433	2.498	169.91
O2-H2A···O2	Expt.	1.02	1.468	2.488	135.62
O4-H4A···O2B	DFT	0.993	1.892	2.869	167.26
O4′-H4A′···O2A	DFT	0.990	1.864	2.837	166.87
O4-H4A···O2	Expt.	0.822	2.011	2.824	169.82
O4-H4B···O2B	DFT	0.988	1.985	2.961	168.91
O4′-H4B···O2A	DFT	0.985	1.953	2.929	170.54
O4-H4B···O2	Expt.	0.836	2.059	2.895	177.90
O5-H5A···O2B	DFT	0.996	1.809	2.797	171.42

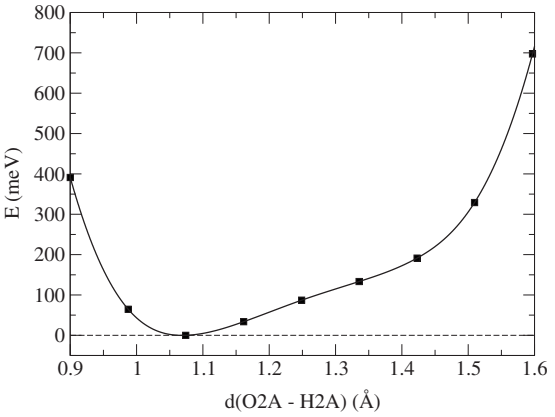

FIG. 4. Energy potential of H2A in the short hydrogen bond O2A-H2A···O2B calculated for the low temperature structure of kanemite.

ture at zero pressure and temperature. In this way we have obtained a single-well, strongly asymmetric hydrogen potential as a function of the O2A-H2A distance (Fig. 4). This result supports the second possibility, namely, that in the ground state ($T=0$, $p=0$), the hydrogen atom is fixed to one of the two experimentally observed sites between the two O2 atoms.

The shape of the potential can be explained by the created structural asymmetry of the crystal caused mainly by the H5A-O5-H5B water molecule, which shifts and creates additional hydrogen bond with O2. The position of the H2A atom is correlated with the orientation of the water molecule, which always makes connection with the oxygen O2B playing the role of acceptor in the O2A-H2A···O2B bond. Thus, the jumping or tunneling of H2A between the two equivalent sites would be possible only with the simultaneous movement of this water molecule. At $T=0$ K, such a sudden position change of the entire molecule is not possible. Moreover, as we discussed in Sec. III A, the symmetry breaking induced by the strong hydrogen bond generates the asymmetry between the A and B tetrahedra, so the hydrogen migration would be necessarily associated with the reorientation of the whole system. To illustrate that such movement is not possible at $T=0$ K, we have estimated the amplitude of the zero-point motion of the H2A atom along the hydrogen bond. It equals to 0.12 Å and it is much smaller than the distance between the two equivalent sites (0.35 Å). Therefore, we conclude that at low temperatures both sites are energetically equivalent, but the proton transfer is not possible and the hydrogen H2A stays in one asymmetric position. With the increasing temperature, the movement of H2A between the two sites can be induced by thermal fluctuations and our further MD studies can reveal the effect of temperature on the behavior of this hydrogen atom.

IV. LATTICE DYNAMICS

In this section, we discuss the spectrum of phonons in kanemite focusing on the vibrations of hydrogen atoms. Since the vibrations in kanemite have very weak dispersion, we analyze only the phonon density of states (PDOS) ob-

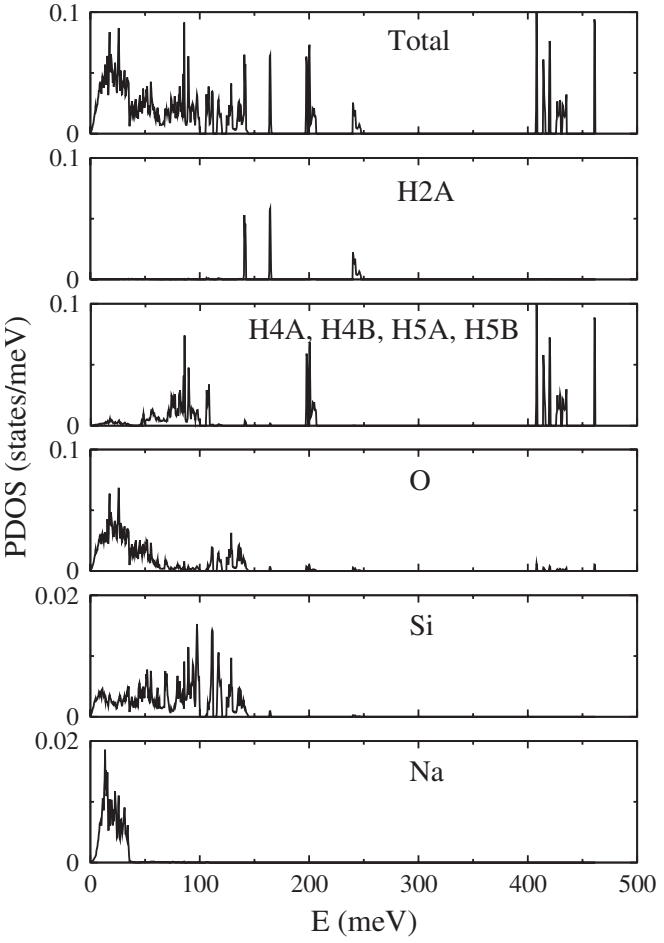

FIG. 5. Total and partial phonon densities of states in kanemite.

tained with 4000 randomly selected k points in the Brillouin zone. The phonon spectrum presented in Fig. 5 can be divided into two regions. The peaks below 150 meV arise due to vibrations of all types of atoms. At higher energies, there are only peaks corresponding to the vibrations of hydrogen atoms, with a small contribution from oxygen and silicon atoms. Because of weak interactions between sodium atoms and other ions, the Na vibrations appear only in the low energy part of the spectrum (<36 meV). It agrees with the spectroscopic assignment of the Na-O stretching modes below 56 meV.[14] The range of energies associated with the vibrations of the silicon atoms is much broader. They extend up to ≈170 meV. Since the calculations were performed for the noncentrosymmetric $Pna2_1$ group, the mutual exclusion rule is not fulfilled and most of the modes can be active in the infrared and Raman spectra. Nevertheless, the assignment of the phonon modes is possible by inspection of the polarization vectors. The energies of selected modes are presented in Table III. According to assignment in Ref. 14, the Raman and infrared bands between 118 and 161 meV correspond to the asymmetric stretching vibrations in the Si-O-Si bridges. We have found the strongest asymmetric vibrations of the Si-O-Si group at 129 meV and weaker at 140 meV. They perfectly correspond to the double peak with intensity maxima at 135 and 145 meV observed in the infrared spec-

TABLE III. Energies (in meV) of selected modes obtained from DFT calculations compared to the Raman and infrared data from Ref. 14.

Mode	DFT	Experiment	Activity
O-H5B stretch	461	444	I
O-H4B stretch	431	429	I
O-H4A stretch	420		
O-H5A stretch	408		
O-H2A stretch	240		
O-H5A(H5B) bend	204	209	I
O-H4A(H4B) bend	198	204	I
O-H2A bend	164		
O-H2A tors	141		
O-H4A(H4B,H5A) tors	79–100		
O-H5B tors	59		
Si-O-Si asym stretch	140	145	I
Si-O-Si asym stretch	129	135	I
Si-O sym stretch		131	R
Si-OH stretch	119	126	R
Si-O-Si sym stretch	81, 90	57–111	R

trum. In the Raman spectrum, there is a strong peak at 131 meV, assigned to the stretching of Si-O bond with one nonbridging oxygen. We have found such mode at lower energies at 119 meV. It can also correspond to broader Raman band centered at 126 meV. The symmetric vibrations of Si-O-Si linkages have lower energies. They were observed between 57–111 meV with a high intensity maximum at 58 meV. We have identified such modes at energies of 81 and 90 meV.

The vibrational movement of hydrogen atoms has in general three characteristic components; O-H bond stretching, *X*-O-H angle bending, and the rotation of O-H bond around a *Y*-*X* bond directly related to the O atom in the concerned O-H bond. The rotational movement can be hampered by crystal field or when a hydrogen bond is being created and small oscillatory (torsional) motion is observed instead. The stretching vibrations appear at higher energies and the torsional vibrations at lower energies than the bending vibrations. The vibrational energies of torsional and stretching modes are very sensitive to presence of hydrogen bonds and therefore they are good indicators of their existence and strength. Creation of a hydrogen bond causes a shift of the OH torsional mode to higher energies and a shift of the OH stretching mode to lower energies. The stronger the hydrogen bond, the greater the energy shifts. The presence of the three components is clearly seen in the partial vibrational spectrum of the atom H2A, which is involved in the short O2-H2A$\cdots$O2 bond (Fig. 5). Its stretching mode has energy equal to 240 meV, and its polarization vector has mainly *z* component. Such a small stretching energy is characteristic for very strong hydrogen bonds. When no hydrogen bond is being created, the O-H stretching modes are observed at much higher energies above 440 meV. In a strong hydrogen bond, the shift of the hydrogen atom toward the acceptor is

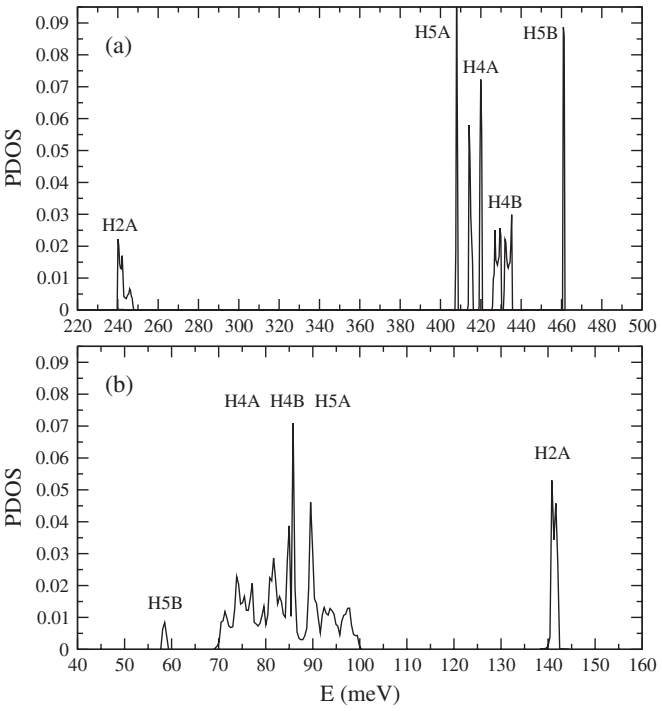

FIG. 6. Energies of the OH (a) stretching and (b) torsion modes for H2A, H4A, H4B, H5A, and H5B hydrogen atoms.

larger than in a weaker one. This strong attraction toward the hydrogen acceptor is accompanied by extreme elongation of the O_{donor}-H bond. Obviously, longer bonding distance corresponds to weaker bond force constant, which is directly related to the vibrational energy of the bond. When comparing the O-H bonding distances (Table II), the values of both experimental and calculated O2A-H2A distances are much larger than the values of the other O-H distances. The hydrogen atoms H4A, H4B, and H5A are bonded in water molecules and involved in moderate hydrogen bonds. Their O-H bond-stretching vibrations are observed in the highest energy range between 408 and 431 meV (Fig. 5). Our calculations show perfect correlation between the OH stretching energies and the donor-acceptor separations in the O-H$\cdots$O bonds. The shortest hydrogen bond corresponds to the lowest OH stretching energy and the longest one to the highest OH stretching energy. The weakest hydrogen bonds present in the structure are thus those involving H4B atom, while stronger involve H4A and H5A. Finally, the strongest hydrogen bond is formed by atom H2A. On the energy scale the O2A-H2A$\cdots$O2B bond is very distinct from the other hydrogen bonds present in the structure, which is indicated by the larger separation of the O2A-H2A stretching energy from the stretching energies associated with the remaining hydrogen atoms. Figure 6(a) nicely shows the three regions, distinguishing the strong (240–250 meV), intermediate (408–431 meV), and no hydrogen bond regions (461 meV). The highest stretching energy in the calculated spectrum (461 meV) belongs to the H5B hydrogen (calculated $d_{\text{O-H5B}}$ $=0.976$ Å) not involved in hydrogen bonding. It can be associated with the intensity maxima observed in the infrared spectra at 444 meV. The very narrow band around 200 meV (Fig. 5), consisting of the bending modes of OH groups as-

sociated with the moderate hydrogen bonds, corresponds very well to infrared results. At energies below 150 meV, there is a wide range of vibrations connected with torsion, wagging, and rocking modes of the water molecules. The peaks corresponding to the OH torsional modes are shown in Fig. 6(b). The lowest energy torsional mode (59 meV) was obtained for hydrogen H5B not involved in hydrogen bonding. The highest energy torsional mode (141 meV) belongs to atom H2A, which is involved in the short strong hydrogen bond O2A-H2A···O2B. Finally, contributions in the central energy region, 70–100 meV, arise due to torsional vibrations of O-H4A, O-H4B, and O-H5A bonds involved in the moderate hydrogen bonds. These torsional modes along with O-H2A bending mode calculated at 141 meV associated with the short hydrogen bond have not been identified in the Raman and infrared studies.

V. CONCLUSIONS

Crystal structure and phonon spectrum of kanemite were studied using the density-functional theory. In our model the crystal *Pbcn* symmetry had to be broken. Choosing a single site for the position of atom H2A, for which two crystallographically equivalent sites are available, the *Pbcn* symmetry was reduced to obtain the highest possible subgroup $Pna2_1$. Our calculations showed that both hydrogen sites are energetically equivalent. However, at low temperatures the H2A atom sits in a single asymmetric potential well, prohibiting it to jump between the two energetically equivalent sides. According to our calculations, atom H2A connects the SiO_4 tetrahedra along the *c* direction by formation of very short O2A-H2A···O2B hydrogen bond ($d_{O\cdots O}$=2.498 Å) in agreement with the experimental observations. The extremely low O2A-H2A stretching energy (240 meV) and high torsional frequency (141 meV) obtained from the PDOS calculations suggest it to be a very strong hydrogen bond—the strongest one found in the structure of kanemite.

Moderate O-H···O hydrogen bonds were found to stabilize the hydrated sodium layers in between the silicon layers with slightly longer O···O distances (Δd_{max}=0.066 Å) in comparison to the experimental data. Apart from the hydrogen bonds reported in the earlier studies, additional O5-H5A···O2B hydrogen bond is recognized to provide a link between the Na layers and the silicon tetrahedra at low temperatures. The bond is created after the whole H5B-O5-H5A water molecule is shifted by 11% along the *b* direction and additionally rotated in the *bc* plane. With the O···O distance equal to 2.797 Å and the OH stretching energy of 408 meV, we define O5-H5A···O2B as a moderate hydrogen bond.

The structural asymmetry, caused by the formation of hydrogen bonds, slightly influences also the geometry of the SiO_4 tetrahedra. Two distinct tetrahedra, one being the donor and the other the acceptor of the strong hydrogen bond O2A-H2A···O2B, are distinguished in the theoretical structure. In the donating tetrahedra, the Si-O2 bond is longer than the Si-O3. The opposite is true in the acceptor tetrahedra, the difference between the Si-O2 and Si-O3 being equal to average of 0.024 Å. Comparing to the experimental structure, there is also larger deformation of the NaO_6 octahedra; instead of three distinct Na-O distances there are six ones in the theoretical model.

These structural modifications due to the symmetry breaking suggest the possibility of a phase transition of the order-disorder type at low temperatures. Such transition would be accompanied by the symmetry reduction of the crystal from the orthorhombic *Pbcn* to one of its subgroup. The $Pna2_1$ space group, used in the present calculations, is one of the candidates for the low-symmetry phase, however, other configurations of protons in the hydrogen bonds O2A-H2A···O2B may also induce different symmetries ($P2_1/c$, $P1$).

ACKNOWLEDGMENTS

The authors thank Z. Olejniczak for valuable discussions. This work was partially supported by Marie Curie Research Training Network under Contract No. MRTN-CT-2006-035957 (c2c) as well as the Polish Government (MNiSW) within Grant No. 541/6.PR UE/2008/7 and the scientific net EKO-KAT.

[1] Z. Johan and G. F. Maglione, Bull. Soc. Fr. Mineral. Cristallogr. **95**, 371 (1972).
[2] A. P. Khomyakov, *Mineralogy of Hyperagpaitic Alkaline Rocks* (Oxford University Press, New York, 1995), p. 223.
[3] G. Perinet, J. J. Tiercelin, and C. E. Barton, Bull. Mineral. **105**, 633 (1982).
[4] K. Beneke and G. Lagaly, Am. Mineral. **62**, 763 (1977).
[5] D. C. Apperley, M. J. Hudson, M. T. J. Keene, and J. A. Knowles, J. Mater. Chem. **5**, 577 (1995).
[6] W. Wieker, D. Heidemann, R. Ebert, and A. Tapper, Z. Anorg. Allg. Chem. **621**, 1779 (1995).
[7] T. Yanagisawa, T. Shimizu, K. Kuroda, and C. Kato, Bull. Chem. Soc. Jpn. **63**, 988 (1990).
[8] S. Inagaki, Y. Fukushima, and K. Kuroda, J. Chem. Soc., Chem. Commun. **1993**, 680.
[9] Y. Sakamoto, S. Inagaki, T. Ohsuna, N. Ohnishi, Y. Fukushima, Y. Nozue, and O. Terasaki, Microporous Mesoporous Mater. **21**, 589 (1998).
[10] F. Kooli, J. Mater. Chem. **12**, 1374 (2002).
[11] E. M. Serwicka and K. Bahranowski, Catal. Today **90**, 85 (2004).
[12] G. G. Almond, R. K. Harris, and K. R. Franklin, J. Mater. Chem. **7**, 681 (1997).
[13] L. A. J. Garvie, B. Devouard, T. L. Groy, F. Camara, and P. R. Buseck, Am. Mineral. **84**, 1170 (1999).
[14] Y. Huang, Z. Jiang, and W. Schwieger, Microporous Mesoporous Mater. **26**, 215 (1998).
[15] M. R. Johnson, K. Parlinski, I. Natkaniec, and B. S. Hudson,

Chem. Phys. **291**, 53 (2003).
[16] F. Fontaine-Vive, M. R. Johnson, G. J. Kearley, J. A. Cowan, J. A. K. Howard, and S. F. Parker, J. Chem. Phys. **124**, 234503 (2006).
[17] M. Sládkovičová, Ľ. Smrčok, P. Mach, D. Tunega, and A. I. Kolesnikov, Chem. Phys. **340**, 245 (2007).
[18] M. Sládkovičová, Ľ. Smrčok, P. Mach, D. Tunega, and A. J. Ramirez-Cuesta, J. Mol. Struct. **874**, 108 (2008).
[19] R. J. Kirkpatrick, A. G. Kalinichev, X. Hou, and L. Struble, Mater. Struct. **38**, 449 (2005).
[20] G. Kresse and J. Furthmüller, Comput. Mater. Sci. **6**, 15 (1996).
[21] P. E. Blöchl, Phys. Rev. B **50**, 17953 (1994); G. Kresse and D. Joubert, *ibid.* **59**, 1758 (1999).
[22] J. P. Perdew, K. Burke, and M. Ernzerhof, Phys. Rev. Lett. **77**, 3865 (1996).
[23] H. J. Monkhorst and J. D. Pack, Phys. Rev. B **13**, 5188 (1976).
[24] K. Parlinski, Z. Q. Li, and Y. Kawazoe, Phys. Rev. Lett. **78**, 4063 (1997).
[25] K. Parlinski, Software PHONON, Cracow (2008).
[26] S. Vortmann, J. Rius, B. Marler, and H. Gies, Eur. J. Mineral. **11**, 125 (1999).